J|A|C|S
ARTICLES
Published on Web 10/19/2006

Electrostatic, Steric, and Hydration Interactions Favor Na^+ Condensation around DNA Compared with K^+

Alexey Savelyev and Garegin A. Papoian*

Contribution from the Department of Chemistry, University of North Carolina at Chapel Hill, Chapel Hill, North Carolina 27599-3290

Received April 27, 2006; E-mail: gpapoian@unc.edu

Abstract: Condensation of monovalent counterions around DNA influences polymer properties of the DNA chain. For example, the Na^+ ions show markedly stronger propensity to induce multiple DNA chains to assemble into compact structures compared with the K^+ ions. To investigate the similarities and differences in the sodium and potassium ion condensation around DNA, we carried out a number of extensive all-atom molecular dynamics simulations of a DNA oligomer consisting of 16 base pairs, $[d(CGAGGTTTAAAC-CTCG)]_2$, in explicit water. We found that the Na^+ ions penetrate the DNA interior and condense around the DNA exterior to a significantly larger degree compared with the K^+ ions. We have provided a microscopic explanation for the larger Na^+ affinity toward DNA that is based on a combination of steric, electrostatic, and hydration effects. Unexpectedly, we found that the Cl^- co-ions provide more efficient electrostatic screening for the K^+ ions than for the Na^+ ions, contributing to the larger Na^+ condensation around DNA. To examine the importance of the discrete nature of water and ions, we also computed the counterion distributions from the mean-field electrostatic theory, demonstrating significant disagreements with the all-atom simulations. Prior experimental results on the relative extent of the Na^+ and K^+ condensation around DNA were somewhat contradictory. Recent DNA compaction experiments may be interpreted to suggest stronger Na^+ condensation around DNA compared to K^+, which is consistent with our simulations. We also provide a simple interpretation for the experimentally observed increase in DNA electrophoretic mobility in the alkali metal series, $Li^+ < Na^+ < K^+ < Rb^+$. We compare the DNA segment conformational preferences in various buffers with the proposed NMR models.

1. Introduction

DNA folds into a highly organized chromatin structure in eukaryotic cells.[1,2] Compacting DNA without charge neutralization is energetically prohibitive,[3] since a double-helix DNA carries two elementary negative charges per base pair. Thus, counterions and the aqueous solvent provide a stabilizing medium for the maintenance of the highly compact and organized DNA structures.[4] In addition, DNA chains possess significant rigidity, resisting bending at scales less than 150 base pairs.[5] Unfavorable bending in the linker DNA, which connects adjacent nucleosomes in a polynucleosomal array, is partially promoted by the positive mobile counterions in an aqueous medium. Therefore, the linker DNA structure, stability, and dynamics are significantly influenced by the composition of the ionic environment and the counterion condensation details. To determine the properties of DNA in various ionic buffers, numerous prior experimental and theoretical studies have examined counterion condensation around DNA, focusing often on sequence-specific details.[6−32] As discussed below, various

(1) van Holde, K. E. *Chromatin*; Springer: New York, 1989.
(2) Alberts, B.; Johnson, A.; Lewis, J.; Raff, M.; Roberts, K.; Walter, P. *Molecular biology of the cell*; Garland Science: New York, 2002.
(3) Schiessel, H. *J. Phys.: Condens. Matter* **2003**, *15*, R699−R774.
(4) Saenger, W. *Principles of nucleic acid structure*; Springer: New York, 1984.
(5) Hagerman, P. J. *Annu. Rev. Biophys. Biophys. Chem.* **1988**, *17*, 265−286.
(6) Shui, X.; Sines, C. C.; McFail-Isom, L.; VanDerveer, D.; Williams, L. D. *Biochemistry* **1998**, *37*, 16877−16887.
(7) Shui, X.; McFail-Isom, L.; Hu, G. G.; Williams, L. D. *Biochemistry* **1998**, *37*, 8341−8355.
(8) Chiu, T. K.; Kaczor-Grzeskowiak, M.; Dickerson, R. E. *J. Mol. Biol.* **1999**, *292*, 589−608.
(9) Tereshko, V.; Minasov, G.; Egli, M. *Nucleic Acids Res.* **1999**, *121*, 3590−3595.
(10) Tereshko, V.; Wilds, C. J.; Minasov, G.; Prakash, T. P.; Maier, M. A.; Howard, A.; Wawrzak, Z.; Manoharan, M.; Egli, M. *Nucleic Acids Res.* **2001**, *29*, 1208−1215.
(11) Bleam, M. L.; Anderson, C. F.; Record, M. T. *Proc. Natl. Acad. Sci. U.S.A.* **1980**, *77*, 3085−3089.
(12) Halle, B.; Denisov, V. P. *Biopolymers* **1998**, *48*, 210−233.
(13) Denisov, V. P.; Halle, B. *Proc. Natl. Acad. Sci. U.S.A.* **2000**, *97*, 629−633.
(14) Hud, N. V.; Feigon, J. *Biochemistry* **2002**, *41*, 9900−9910.
(15) Marincola, F. C.; Denisov, V. P.; Halle, B. *J. Am. Chem. Soc.* **2004**, *126*, 6739−6750.
(16) Korolev, N.; Lyubartsev, A. P.; Rupprecht, A.; Nordenskiold, L. *Biophys. J.* **1999**, *77*, 2736−2749.
(17) Korolev, N.; Lyubartsev, A. P.; Rupprecht, A.; Nordenskild, L. *Biopolymers* **2001**, *58*, 268−278.
(18) Manning, G. S. *J. Chem. Phys.* **1969**, *51*, 924−933.
(19) Manning, G. S. *Q. Rev. Biophys.* **1978**, *11*, 179−246.
(20) Shklovskii, B. I. *Phys. Rev. Lett.* **1999**, *82*, 3268−3271.
(21) Naji, A.; Netz, R. R. *Eur. Phys. J. E: Soft Matter* **2004**, *13*, 43−59.
(22) Lee, K.-C.; Borukhov, I.; Gelbart, W. M.; Liu, A. J.; Stevens, M. J. *Phys. Rev. Lett.* **2004**, *93*, 128101.
(23) Angelini, T. E.; Liang, H.; Wriggers, W.; Wong, G. C. L. *Proc. Natl. Acad. Sci. U.S.A.* **2003**, *100*, 8634−8637.
(24) Fuoss, R. M.; Katchalsky, A.; Lifson, S. *Proc. Natl. Acad. Sci. U.S.A.* **1951**, *37*, 579−589.
(25) Shkel, I. A.; Tsodikov, O. V.; Record, M. T. *Proc. Natl. Acad. Sci. U.S.A.* **2002**, *99*, 2597−2602.
(26) Deshkovski, A.; Obukhov, S.; Rubinstein, M. *Phys. Rev. Lett.* **2001**, *86*, 2341−2344.
(27) Cheatham, T. E.; Young, M. A. *Biopolymers* **2000**, *56*, 232−256.

10.1021/ja0629460 CCC: $33.50

experimental results on the relative extent of the Na^+ and K^+ condensation around DNA are contradictory. In this work, we carried out all-atom molecular dynamics (MD) simulations of a 16-mer DNA, $[d(CGAGGTTTAAACCTCG)]_2$, in explicit water with Na^+ and K^+ counterions to gain insight into more generic aspects of monovalent counterion distribution around the whole DNA molecule, defocusing from the sequence-specific details.

Sequence-dependent DNA hydration and ionic binding were studied with X-ray crystallography[6−10,33] and solution techniques, including NMR.[11−15] Dickerson and co-workers[33] determined the crystal structure of a specific B-DNA 12-mer, known in the literature as the Drew−Dickerson dodecamer. This study confirmed that the aqueous/salt environment substantially influences the DNA conformational preferences.[33] Subsequent crystallographic papers[6−10] focused on determining whether the counterions reside in the minor groove of the DNA central A-tract. Some difficulties in distinguishing among Na^+ ions and water, partial localization of heavier alkali metal ions (K^+, Rb^+), and a possible shift of the energy/entropy balance of ion−water substitution caused by the cryogenic temperatures used in recent crystallographic works have led to disagreements over interpretation of the obtained results.[6−8] Intrusion of the cations into the minor groove was investigated in complementary NMR studies. In particular, long residence times were found for monovalent cations bound to specific DNA sites.[13,15] Competitive binding of various cations to specific DNA sites was also studied by NMR techniques.[13,15] When the K^+ and Na^+ ions were compared, the K^+ ions were found to have a slightly higher affinity toward binding to the DNA minor groove than the Na^+ ions.[11,13]

Another set of experimental papers focused on the macroscopic properties of the DNA chains in various ionic buffers. Specifically, the influence of different monovalent cations on DNA mobility in free solution was studied recently by capillary electrophoresis.[34] Among the first-group monovalent cations, the measured DNA electrophoretic mobilities increased down the group, $Li^+ < Na^+ < K^+ < Rb^+$, for single- and double-stranded DNA segments.[34] This trend has been partially rationalized on the basis of the ion-specific nonequilibrium relaxation effect, which reduces DNA mobility due to polarization of the counterionic atmosphere by the external electric field.[35,36] The tendency of various ions to alter water hydrogen-bonded structure, changing the viscosity, has also been suggested to play an important role.[34] In addition to these effects, we speculate that lower DNA mobility in the Na^+ buffer indicates more efficient DNA chain charge neutralization by the Na^+ ions, compared with the K^+ ions. This, in turn, suggests that the DNA binding propensities among the first-group cations follow the trend $Li^+ > Na^+ > K^+ > Rb^+$. Since this is opposite to the trends obtained from the recent NMR studies,[13] one might infer that preferential counterion binding to the DNA minor grooves may not determine the overall charge neutralization of the whole DNA chain.

In a different set of experiments, long DNA chain compaction, induced by various monocations, was monitored by fluorescent microscopy.[37−39] It was reported recently that DNA condensation was mediated more significantly by Na^+ compared to K^+.[39] It should be noted, however, that the primary DNA compactor in the above experiment was the neutral poly(ethylene glycol) (PEG), used to mimic the crowded environment inside the living cell. Nevertheless, unequal concentrations of the added monovalent salts, NaCl or KCl, were then necessary to induce the DNA collapse. We speculate that stronger counterion condensation reduces electrostatic repulsion among DNA chains, thus facilitating PEG-induced compaction. Since NaCl showed the highest activity among the studied salts, this argument suggests stronger Na^+ condensation around DNA, in agreement with our interpretation of the electrophoretic mobility results. In yet another series of experimental publications on competition among mono-, di-, and trivalent inorganic ions for association with oriented DNA fibers, lack of significant DNA selectivity toward the Na^+ or K^+ ions was found.[16,17] Thus, various experimental results on the relative extent of the Na^+ and K^+ condensation around DNA are not in complete agreement with each other.

Numerous theoretical treatments of the counterion distribution around DNA were based on the combination of the counterion condensation (CC) model and the Poisson−Boltzmann (PB) mean-field electrostatics. In a seminal work, Onsager and Manning[18] demonstrated that CC must occur on linear rods that are uniformly charged above some critical charge density. The DNA molecule, being linear and carrying high charge per unit length, is well above this threshold.[40] One can estimate from these simple arguments that 76% of the total DNA charge is expected to be neutralized by condensed counterions within a 9 Å Manning radius.[19,41] CC results in significant restriction of the counterion movement near DNA. In addition, significant dynamical correlations are generated among the condensed counterions.[20] These correlations may, under certain circumstances, produce nontrivial effects, such as an attraction between the macro-ions of the same charge.[20−23] CC reduces the total charge of the macromolecule to such a level that it might become more appropriate to treat the rest of the ions within a continuum mean-field approach. In this way, the diffuse ionic atmosphere beyond ∼10 Å from the DNA surface may be described with the PB equation, a theory based on approximating the water with a continuum dielectric and ignoring the discrete nature of ions.[42]

When simplified models of DNA and its ionic environment are used, the former is usually treated as a uniformly charged cylinder surrounded by counterions only, without a corresponding salt, in a continuum dielectric medium.[24] In general, this salt-free solution may not represent the real systems at physiological salt concentrations. A complete asymptotic solution of the cylindrical PB equation at experimental salt concentrations

(28) Cheatham, T. E.; Kollman, P. A. *Annu. Rev. Phys. Chem.* **2000**, *51*, 435−471.
(29) Egli, M. *Chem Biol* **2002**, *9*, 277−286.
(30) Rueda, M.; Cubero, E.; Laughton, C. A.; Orozco, M. *Biophys. J.* **2004**, *87*, 800−811.
(31) Ponomarev, S. Y.; Thayer, K. M.; Beveridge, D. L. *Proc. Natl. Acad. Sci. U.S.A.* **2004**, *101*, 14771−14775.
(32) Varnai, P.; Zakrzewska, K. *Nucleic Acids Res.* **2004**, *32*, 4269−4280.
(33) Wing, R.; Drew, H.; Takano, T.; Broka, C.; Tanaka, S.; Itakura, K.; Dickerson, R. E. *Nature (London)* **1980**, *287*, 755−758.
(34) Stellwagen, E.; Dong, Q.; Stellwagen, N. C. *Biopolymers* **2005**, *78*, 62−68.
(35) Manning, G. *J. Phys. Chem.* **1981**, *85*, 1506−1515.
(36) Stellwagen, E.; Stellwagen, N. C. *Biophys. J.* **2003**, *84*, 1855−1866.
(37) Mayama, H.; Iwataki, T.; Yoshikawa, K. *Chem. Phys. Lett.* **2000**, *318*, 113−117.
(38) Mayama, H.; Yoshikawa, K. *Macromol. Symp.* **2000**, *160*, 55−60.
(39) Zinchenko, A. A.; Yoshikawa, K. *Biophys. J.* **2005**, *88*, 4118−4123.
(40) Manning, G. S. *J. Am. Chem. Soc.* **2003**, *125*, 15087−15092.
(41) Deserno, M.; Holm, C.; May, S. *Macromolecules* **2000**, *33*, 199−206.
(42) Honig, B.; Nicholls, A. *Science* **1995**, *268*, 1144−1149.

was recently obtained,[25] however, at infinite dilution of the polyion. The latter regime is another obstacle in direct application of the theory to real systems, such as a DNA solution having a finite DNA concentration. The polyion concentration effect was investigated in detail by Rubinstein and co-workers[26] for various regimes of moderately dilute polyelectrolyte solutions, arriving at different power laws for the counterion distribution as a function of the distance from the polyion surface, depending on the polyion concentration.

A more realistic picture of DNA−counterion interactions has emerged from all-atom MD simulation of DNA in explicit water at physiological salt concentrations. In particular, most of the recent studies,[30−32,43−45] motivated by the prior crystallographic and NMR works, investigated in great detail sequence-specific DNA hydration, sequence-specific counterion binding, and associated local modulation of the DNA structure (more details and numerous additional citations are given in recent reviews[27−29]). Most prior all-atom MD simulations were carried out with buffers composed of a single salt, such as a NaCl solution. A few simulation papers comparing the condensation of Na^+, K^+, and other alkali metal ions showed that they differ substantially in their interactions with the DNA sites.[46,32] In particular, Na^+ and K^+ were found to reside mainly in the minor and major grooves, respectively, and a detailed analysis of the specific interactions in these regions was presented.[32] However, one is also interested in the larger picture of the counterion condensation around DNA, ignoring the sequence details. As mentioned earlier, the electrophoretic measurements of the DNA mobility[34] may be interpreted to suggest that the overall DNA charge neutralization may not be inferred from the preferential binding to specific DNA sites, such as to the minor groove. Another issue which did not attract significant attention is the competitive distribution of two monovalent cations around DNA. This is an important consideration, since different cations were shown to have different effects on the formation of compact and highly organized chromatin structures.[47]

In this paper, we present a comprehensive comparative analysis of the Na^+ and K^+ condensation around DNA, focusing on DNA as a single polyanion. We chose a 16-base-pair DNA oligomer, $[d(CGAGGTTTAAACCTCG)]_2$, which was a subject to structural studies in a recent NMR work.[48] We studied this 16-mer in various buffers with different ionic compositions (Na^+/NaCl, K^+/KCl, and their mixture) using all-atom MD simulations with explicit water, as elaborated in the Computational Methods section. The 16-mer considered in this work is longer than the DNA oligomers that were studied in the prior works[30−32] (see also refs 27, 28, and references therein). Our MD results are among the most extensive DNA simulations reported to date. On the basis of these simulations, we present a simple picture of how the counterions distribute at distances up to 15 Å from the DNA surface and how these distributions compare with the mean-field electrostatic calculations. To explain the observed dramatic difference in the propensity for the Na^+ and K^+ ions to penetrate the DNA interior and to condense around the DNA exterior, we suggest the following three mechanisms of how the ion size regulates counterion condensation: (1) Na^+ ions, because of their smaller size, better fit into the *DNA core* binding pockets; (2) Na^+ ions experience larger, attractive electrostatic potential near the DNA exterior surface because they approach closer to the surface; and (3) because of a lower dehydration penalty for large K^+ ions, which have smaller charge density, very extensive $K^+ - Cl^-$ clustering is observed, as opposed to the absence of clustering for the Na^+ ions. This, in turn, leads to less efficient screening of Na^+ counterions by the Cl^- co-ions. Each of these effects promotes higher Na^+ condensation around DNA compared to K^+, thus resulting in a significant overall difference. Finally, the DNA conformational behavior in various buffers is analyzed and compared with the published NMR models.[48] Our simulations suggest that Na^+ condenses more strongly around DNA, resulting in larger charge neutralization, which, in turn, might lead to lower electrophoretic mobility and larger tendency to compact the DNA chain.

2. Computational Methods

2.1. MD Simulation Protocol. The starting point for all simulations was a canonical B-form of a 16-base-pair DNA oligomer, $[d(CGAGGTTTAAACCTCG)]_2$.[48] We built an ideal DNA chain model and carried out all-atom MD simulations in explicit, TIP3P water[49] using the AMBER 8.0 suite of programs[50] and the Amber Parm99 force field.[51] To address a specific nature of the interactions between DNA and two monovalent cations, Na^+ and K^+, four MD simulations with different compositions of the neutralizing Na^+ and/or K^+ ions and the corresponding extra NaCl and/or KCl salts were performed. The initial positions of the ions were determined from the computed electrostatic potential using LEaP.[50] The following systems were prepared: (1) 30 neutralizing Na^+ ions and ∼0.12 M of extra NaCl salt (14 additional Na^+ and Cl^- ions); (2) 30 neutralizing K^+ ions and ∼0.12 M of extra KCl salt (14 additional K^+ and Cl^- ions); (3) a mixture of 15 neutralizing Na^+ and 15 neutralizing K^+ ions and additional ∼0.06 M of both NaCl and KCl salts (7 additional Na^+ ions, 7 additional K^+ ions, and 14 Cl^- ions); and (4) a mixture of 15 neutralizing Na^+ ions and 15 neutralizing K^+ ions only (without extra salts). Henceforth, we shall refer to the above simulations as **1**, **2**, **3**, and **4**, respectively. The DNA oligomer and the ions were further solvated in more than 6000 TIP3P water molecules in a rectangular box, having dimensions 50 × 50 × 86 Å. Two DNA segments from neighboring periodic images were at least 30 Å apart. The overall number of atoms was ∼19 500 in the periodic box. We used a multistage equilibration process, reported by Orozco and co-workers,[52] to equilibrate all starting structures. The subsequent production runs for each MD in **1**−**4** were carried out at constant temperature (300 K) and pressure (1 bar) using the Langevin temperature equilibration scheme (see AMBER 8 manual), the "weak-coupling" pressure equilibration scheme,[53] and periodic boundary conditions. To test how these results compare with those of other commonly used temperature equilibration techniques, we repeated simulation **3** with the Berendsen temperature coupling algorithm. The obtained counterion−DNA radial distribution functions (see next

(43) Feig, M.; Pettitt, B. M. *Biophys. J.* **1999**, *77*, 1769−1781.
(44) McConnell, K. J.; Beveridge, D. L. *J. Mol. Biol.* **2000**, *304*, 803−820.
(45) Hamelberg, D.; McFail-Isom, L.; Williams, L. D.; Wilson, W. D. *J. Am. Chem. Soc.* **2000**, *122*, 10513−10520.
(46) Lyubartsev, A. P.; Laaksonen, A. *J. Biomol. Struct. Dyn.* **1998**, *16*, 579−592.
(47) Strick, R.; Strissel, P. L.; Gavrilov, K.; Levi-Setti, R. *J. Cell Biol.* **2001**, *155*, 899−910.
(48) McAteer, K.; Aceves-Gaona, A.; Michalczyk, R.; Buchko, G. W.; Isern, N. G.; Silks, L. A. P.; Miller, J. H.; Kennedy, M. A. *Biopolymers* **2004**, *75*, 497−511.
(49) Miyamoto, S.; Kollman, P. A. *J. Comput. Chem.* **1992**, *13*, 952−962.
(50) Case, D.; Cheatham, T.; Darden, T.; Gohlke, H.; Luo, R.; Merz, K.; Onufriev, A.; Simmerling, C.; Wang, B.; Woods, R. *J. Comput. Chem.* **2005**, *26*, 1668−1688.
(51) Wang, J.; Cieplak, P.; Kollman, P. *J. Comput. Chem.* **2000**, *21*, 1049−1074.
(52) Shields, G. C.; Laughton, C. A.; Orozco, M. *J. Am. Chem. Soc.* **1998**, *120*, 5895−5904.
(53) Berendsen, H. J.; Postma, J. P.; van Gunsteren, W. F.; DiNola, A.; Haak, J. R. *J. Chem. Phys.* **1984**, *81*, 3684−3690.

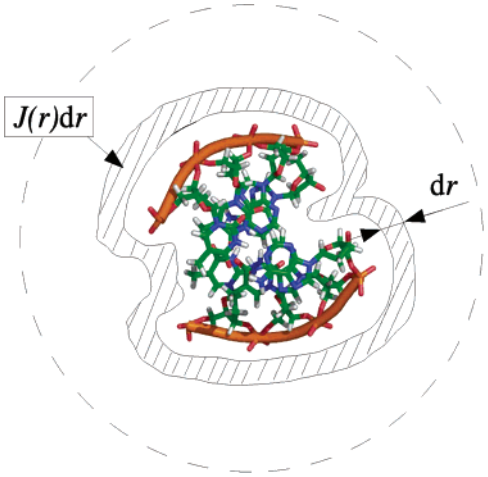

Figure 1. Top view of the DNA and an equidistant shell from its surface (dashed region).

subsection) were identical to those obtained using Langevin dynamics. Harmonic positional restraints of 5×10^{-5} kcal/mol·Å^2 were applied to all DNA atoms to prevent a large angle rotation of the macromolecule in the anisotropic simulation box, which, in turn, would have lowered the separation among DNA segments in neighboring periodic cells. These restraints were extremely weak, allowing atomic thermal fluctuations on the order of ~10 Å around the reference atomic positions; thus, they did not influence the conformational dynamics of the stiff DNA oligomer.

The translational center-of-mass motion was removed every 2 ps. We used the SHAKE algorithm[54] to constrain all bonds involving hydrogens, allowing us to perform all MD simulations with an increased time step of 2 fs without any instability. The particle mesh Ewald method[55] was used to treat long-range interactions with a 9 Å nonbonded cutoff. The production runs for simulations **1**, **3**, and **4** were carried out for 60 ns to ensure the equilibration of ions. It was shown in prior works[31,32] that 50 ns MD was enough to equilibrate the Na^+ atmosphere around DNA in a smaller system comprised of ~16 000 atoms. Given the slightly larger size of our system (~19 500 atoms), we used extra 10 ns of MD to ensure equilibration. The production run for simulation **2** was carried out for only 30 ns, since it was shown previously that the equilibration of the K^+ ions was twice as fast as that of the Na^+ ions.[32]

2.2. Analysis of Counterion Distribution around DNA. To analyze in detail the Na^+ and K^+ distributions around the DNA segment, we calculated their radial distribution functions (RDFs).[56] All DNA−counterion RDFs were based on first defining the DNA−counterion distance as the closest distance between the DNA molecule and the particular counterion. These distances were used to construct DNA−ion distance histograms from each snapshot of the MD simulation. To obtain the RDFs, the histograms need to be normalized by the volume Jacobian.[56] Indeed, the number of neighbors within a distance r from a given object is

$$n(r) = \rho \int_0^r g(r)\, J(r)\, \mathrm{d}r \qquad (1)$$

where ρ is the average particle concentration, $g(r)$ is the RDF (pair correlation function), and $J(r)$ is the volume Jacobian. We defined the latter as the volume of a shell, equidistant from the DNA surface (see Figure 1). The volume Jacobian was numerically calculated as a function of a distance from the DNA surface (Figure 2a). A similarly

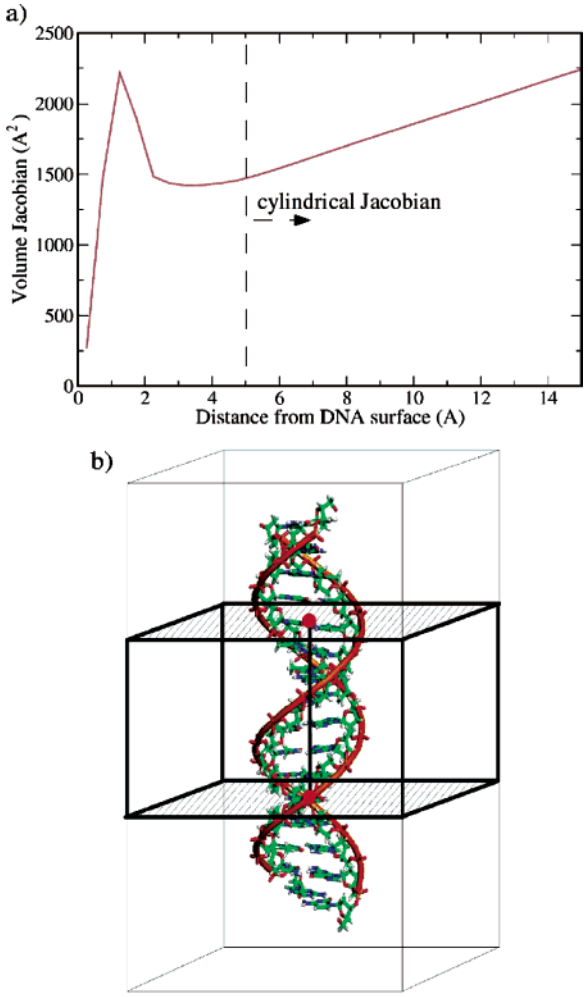

Figure 2. (a) Numerical DNA volume Jacobian as a function of the distance from the DNA surface. It is seen that only after 5 Å from DNA, the function is monotonically increasing and can be approximated by the cylindrical Jacobian. (b) The ionic distribution was analyzed in the boxed region to minimize the end effects.

defined volume Jacobian was used for the ion−DNA RDF normalization in ref 43. The present method of computing $J(r)$ differs from the standard procedure of calculating either the spherical (see *ptraj* utility of the AMBER package) or the cylindrical Jacobian (as used in ref 31).

Although DNA is, on average, cylindrically symmetric and the use of the cylindrical Jacobian is reasonable, the latter techniques lead to an overestimation of the counterion condensation at small distances from the DNA surface. This is important, in particular, when calculating the absolute number of ions contributing to the various RDF peaks and subsequently determining the fraction of the DNA charge neutralized by condensed counterions (see below). The numerical volume Jacobian, taking into account the complex and irregular shape of the DNA segment (see Figure 1), is characterized by an unusual *non-monotonic* behavior in the vicinity of the DNA oligomer (Figure 2a). It is seen that only at distances more than ~5 Å from DNA surface can the monotonically increasing Jacobian be approximated by the cylindrical one. Since DNA is a relatively rigid macromolecule, we calculated the volume Jacobian every 100 time steps. Ion−DNA distance histograms, computed over the MD simulation course for every snapshot, were normalized by the corresponding numerical Jacobian. Three-dimensional grids with lattice spacings of 0.5 and 0.25 Å were used to calculate the ion−DNA distance histograms and the volume

(54) Ryckaert, J.-P.; Ciccotti, G.; Berendsen, H. J. *J. Comput. Phys.* **1977**, *23*, 327−341.
(55) Darden, T.; York, D.; Pedersen, L. *J. Chem. Phys.* **1993**, *98*, 10089−10092.
(56) Barrat, J.-L.; Hansen, J.-P. *Basic concepts for simple and complex liquids;* Cambridge University Press: Cambridge, UK, 2003.

Jacobians, respectively. The biochemical algorithm library (BALL)[57] was used to implement the computational analysis subroutines.

To minimize the end effects, only the inner fraction of the DNA segment (eight internal base pairs) was used for computing the RDFs. This was achieved by "clipping" the periodic boundary cell with two parallel planes that pass through the centers of the upper and lower halves of the DNA oligomer and perpendicular to the line connecting these centers (Figure 2b). The above procedure was repeated for each snapshot along the MD trajectory.

2.3. Comparing the Ionic Charge Densities with Mean-Field Electrostatic Calculations. To compare our results from the all-atom explicit water MD simulations with the conventional electrostatic picture, we numerically solved the nonlinear Poisson−Boltzmann equation with the adaptive Poisson−Boltzmann solver (APBS)[58] to find the ionic charge density around the all-atom DNA oligomer. A grid of 193, 193, and 353 lattice points in x, y, and z directions, respectively, was used to ensure approximately the same 0.25 Å spacing used for calculation of the volume Jacobian. Both the ion−DNA distance histograms, computed from the charge density using the lattice spacing of 0.5 Å, and the volume Jacobian were obtained using the technique described in the preceding section. A standard value of 1.4 Å was used for the solvent probe radius. The solute and solvent dielectric constants were set to 2 and 78, respectively. These results were insensitive to the exact value of the solute dielectric constant. For example, calculations with a dielectric constant of 4 produced virtually identical charge distributions. The values for the mobile ion species' radii were taken from the AMBER parm99 force field used in MD simulations. We used multiple Debye−Hückel boundary conditions (DHBCs) for the electric potential.[58] This results in the potential at the far boundary being equal to the values prescribed by a Debye−Hückel model for multiple, non-interacting spheres with point charges. DHBCs provided better results than the zero-field boundary conditions, resulting in a much smaller numerical error. It is important to note that DHBCs, which are commonly used, are not equivalent to the periodic boundary conditions in the sense that the ions are not confined within a specified volume around DNA. This leads to a "charge leakage" from the volume of interest, corresponding to the periodic boundary cell in the MD simulations. The above effect is entropic in nature (see, e.g., ref 26). Because of the counterion escape, c_{PB} was found to be less than c_{MD}, where c_{PB} and c_{MD} are the average counterion charges in the PB and the MD simulation boxes, respectively. To facilitate the comparison of the RDFs, each RDF resulting from the PB solution was uniformly rescaled as $g'_{PB}(r) = (c_{PB}/c_{MD})g_{PB}(r)$.

2.4. Analysis of the Water Shell around the Counterions. To investigate how the discreteness of water and ions influences the character of Na^+ and K^+ distributions around the DNA molecules, we analyzed the first solvation shell water molecules around the counterions. To determine the radius of the first solvation shell, we used the corresponding counterion−water RDFs, built from independent MD simulations of an electroneutral system consisting of Na^+/K^+ and Cl^- ions solvated in water. For each simulation, we generated a histogram of the average number of water molecules within the counterion's first solvation shell as a function of the counterion distance from the DNA surface.

2.5. Analysis of Counterion−Co-ion Clusters. Interactions between the mobile counterions (Na^+, K^+) and the mobile co-ions (Cl^-) during the course of the MD simulations appeared to be of primary importance for the interpretation of the obtained results. Ionic clusters of various size and composition were formed and re-formed, which in turn influenced the different extents of the condensation of Na^+ and K^+ ions around the DNA oligomer. Therefore, we investigated first how the cluster distribution for Na^+ and K^+ depends on the buffer composition. Next, we looked in detail at the average numbers of both

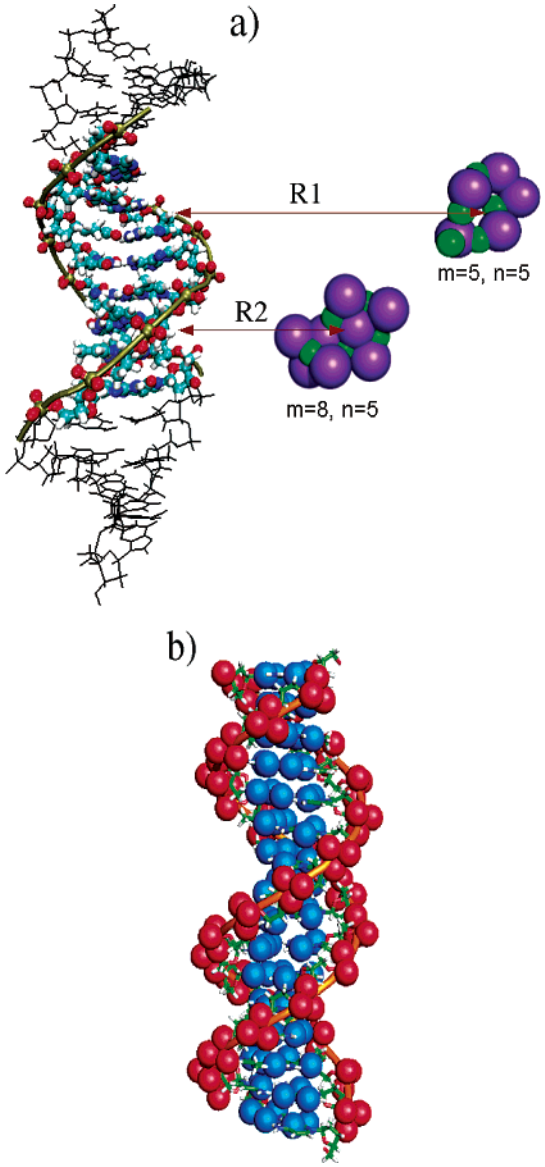

Figure 3. (a) Schematic illustration of the $K^+_mCl^-_n$ cluster distribution around the inside eight base pairs of the DNA (depicted in color). Here, m and n are the numbers of K^+ (blue) and Cl^- (green) ions in a cluster, respectively. As will be discussed later, due to electrostatic attraction, clusters with $m > n$ composition tend to be closer to the DNA surface than those with equal ($m \approx n$) numbers of both K^+ and Cl^- atoms ($R1 > R2$). (b) The most prevalent DNA binding sites for Na^+ and K^+ ions. The sites are partitioned into the *interior* (blue) and the *exterior* (red). The corresponding DNA atoms are N7,N3,O2,O6,O4 (blue) and O1P,O2P,O3* (red).

counterions and co-ions participating in a cluster as a function of the distance between the cluster center and the DNA surface (see Figure 3a). We calculated the distribution of cluster charge around DNA, which helped to rationalize the nontrivial shape of the Cl^-/DNA RDF in systems with high clustering (see below). Both procedures were carried out by calculating the average number of counterions in clusters formed by counterions and co-ions in each system. For example, if a Na^+ ion and a Cl^- ion were found to be at a distance of less than 3.7 Å, then they were considered to belong to the same cluster. For the K^+ and Cl^- pair, a distance threshold of 5.3 Å was used. The numerical values of the corresponding distance thresholds were estimated as the sum of the ionic radii of the corresponding ions, Na^+ and K^+.

2.6. Analysis of DNA Binding Sites. Since the conventional electrostatic picture fails to describe direct binding (as discussed below), we analyzed in more detail how counterions penetrate the DNA core and bind to the DNA exterior. First, we defined a direct interaction

(57) Kohlbacher, O.; Lenhof, H. P. *Bioinformatics* **2000**, *16*, 815−824.
(58) Baker, N. A.; Sept, D.; Joseph, S.; Holst, M. J.; McCammon, J. A. *Proc. Natl. Acad. Sci. U.S.A.* **2001**, *98*, 10037−10041.

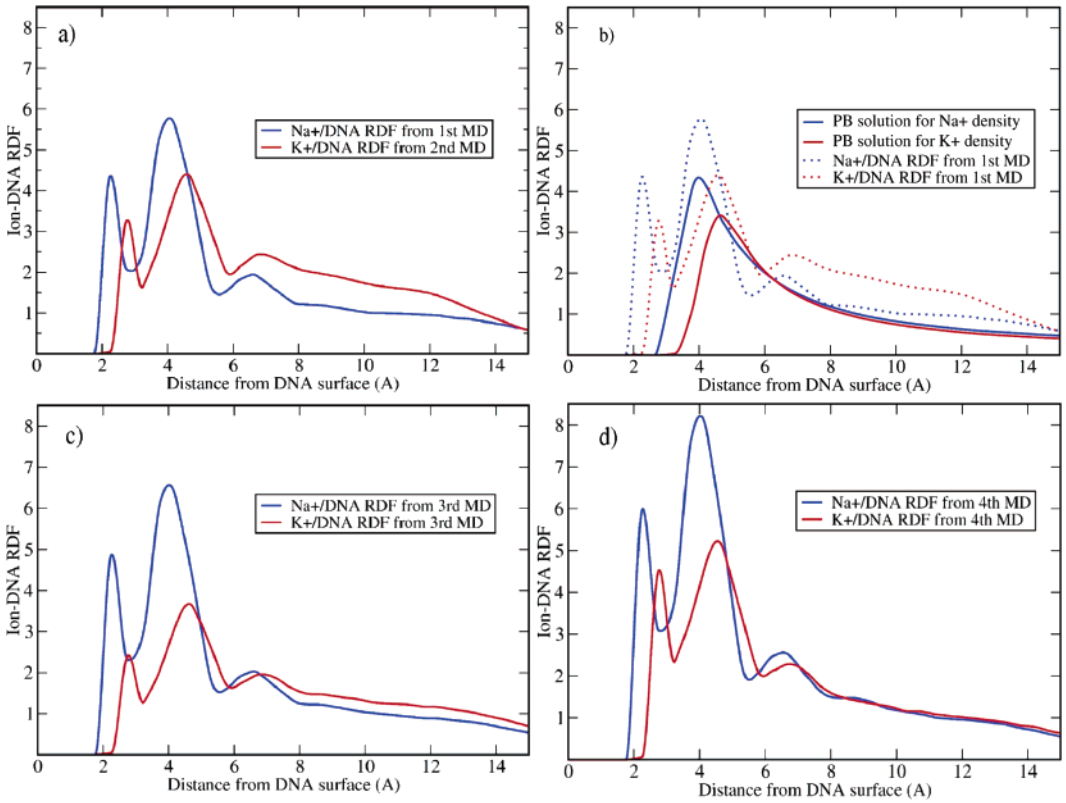

Figure 4. Na^+/DNA (blue) and K^+/DNA (red) RDF from (a) simulations **1** and **2**, corresponding to simple Na^+/NaCl and K^+/KCl compositions; (b) numerical solution of the PB equations, scaled as explained in the Computational Methods section; (c) simulation **3**, corresponding to a 1:1 mixture of Na^+/K^+ counterions and NaCl/KCl salts; and (d) simulation **4**, with the same as in the third MD 1:1 mixture of Na^+/K^+ ions, but without salt (no chlorides).

between a DNA atom and a counterion if the corresponding distance is less than 2.75 Å for Na^+ and 3.25 Å for K^+ ions. These values correspond to the first minimum in the DNA−counterion RDFs, separating the first peak, which characterizes direct binding, from the second peak, corresponding to water-mediated interactions. From the detailed analysis of the *most prevalent* DNA binding sites (see the Supporting Information), we partitioned the DNA atoms into *external* and *internal* sites in Figure 3b. The first-group atoms are located in the outer regions of the polyion, near the phosphorus atoms, and are easily accessible to counterions. This group is comprised of the O1P, O2P, and O3* atoms, where all atom definitions are in accordance with the AMBER force field notation. The internal group includes the N7, N3, O2, O6, and O4 DNA atoms, which are primarily located close to the longitudinal axis of the oligomer (Figure 3b). Since they are buried inside the DNA core, the larger K^+ and the smaller Na^+ ions showed different tendencies to penetrate between the DNA strands and to interact with the internal and external sites. While counterion binding to the external DNA sites is presumably more electrostatic in nature, binding to the internal sites is reminiscent of chemisorption.

3. Results and Discussion

3.1. Comparing the Counterion Distribution from the MD and the Mean-Field Electrostatics. The counterion−DNA RDFs, properly normalized by the numerical volume Jacobians (see the Computational Methods section), show the likelihood for a counterion to be at a particular distance from the DNA surface. The analysis of the RDFs for pure Na^+ (simulation **1**) and pure K^+ (simulation **2**) buffers revealed that the sodium ion condensation is significantly larger in the immediate vicinity of the DNA chain than that of the potassium ions. This is illustrated, in particular, by the amplitudes of the first and second peaks in the counterion−DNA RDFs (Figure 4a). On the other hand, at DNA−counterion distances of more than 5 Å, which corresponds to the third RDF peak and beyond, the K^+ ions were found more frequently than the Na^+ ions. Since the total numbers of sodium and potassium counterions in the simulation box are equal, it is expected that stronger Na^+ condensation around the DNA vicinity would result in relative Na^+ depletion in box regions far from DNA. Therefore, the main observation to be rationalized is the more pronounced tendency for Na^+ to condense around DNA.

To explore this issue, it is appropriate to compare first the above RDFs with the mean-field PB theory results. The latter calculations provide an additional insight into whether the observed distributions are in agreement with the conventional electrostatic picture. The numerical solutions of the nonlinear PB equations for two systems with ionic/salt composition corresponding to MDs **1** and **2** produced specific Na^+ and K^+ charge densities, shown in the form of the DNA−counterion RDFs in Figure 4b. A qualitative difference among the mean-field PB RDFs and the MD simulation RDFs is apparent and, indeed, not surprising, since the discrete nature of both counterions and water is ignored in the continuum mean-field electrostatics. The peaks in the all-atom RDFs show a formation of ionic "shells" around the polyion. The peak in the RDFs obtained from the PB solutions correspond to the second peak in the all-atom RDF, which, in turn, arises from the combination of electrostatic and water-mediated DNA−counterion interactions. However, the PB RDFs completely lack the first peaks in the all-atom RDFs (Figure 4b). The latter corresponds to direct binding between the counterions and the DNA, where ions partially penetrate the DNA core (atoms depicted in blue in

Figure 3b). Thus, the nature of these interactions is not purely electrostatic but has an additional chemisporption component.

It was shown in prior works that the counterion condensation details were important in determining the extent of DNA compaction.[37−39] Stronger sodium condensation around DNA (Figure 4a) results in more significant short-range DNA charge neutralization and a stronger propensity to induce DNA compaction. This conclusion is in agreement with recent experimental results on DNA compaction.[39] A simple solution of the PB equation would not distinguish between the Na^+ and K^+ ions, since the counterion size does not enter into the nonlinear PB equation. Furthermore, due to the nature of the Coulomb law, the counterion density becomes unrealistically high near the polyion surface. Thus, an ad-hoc solution to this problem is to introduce a cutoff distance from the DNA surface, based on atomic radii, such that the charge density is set to zero in the regions close to the DNA surface.[58] Consequently, the corresponding numerical solution of the PB equation also predicts a stronger tendency for the Na^+ ions to interact with the DNA oligomer (Figure 4b). The smaller Na^+ size allows a closer approach of the counterion to the DNA surface, resulting in the larger amplitude peak in the DNA−Na^+ RDF compared with the DNA−K^+ RDF (Figure 4b). On the other hand, the counterion−DNA RDFs for both Na^+ and K^+ nearly coincide beyond 6 Å from the DNA surface and exhibit an exponential decay. As can be seen from Figure 4b, this behavior is different from the all-atom MD behavior, which predicts that K^+ ions dominate at distances >5 Å from the DNA surface.

The discrepancy between the *long-range* parts of the RDFs obtained from the all-atom MD simulations and those obtained from the PB calculations may be traced to different regimes of the polyion dilution in these calculations. In particular, one DNA segment is immersed in an infinitely large salt buffer in the PB calculation, corresponding to an infinitely dilute DNA solution. In our system, the DNA concentration in all-atom MD was ∼8 mM. Since the mobile ions are confined within the periodic boundary cell in the MD simulations, the net charge of the all-atom system is zero in the periodic cell. On the other hand, the net charge of the same region in the PB system was nonzero, as a result of a "charge leakage" from the PB cell (see the Computational Methods section). The entropy of counterions being delocalized beyond this region is sufficient to overcome the electrostatic attraction of DNA and allow them to escape the polyion vicinity.[26]

Counterion distribution around cylindrical counterions was investigated using the PB equation by Rubinstein and co-workers;[26] however, their investigation was done in a salt-free regime. Following their classification, PB distributions in Figure 4b correspond to the regime of *saturated* condensation, when the polyion charge is almost completely compensated by the counterions within the cell. In this regime, the uncondensed counterions are self-similarly distributed throughout the cell, according to the power law $c(r) \sim r^{-\gamma}$ ($\gamma = 2$).[26] Indeed, the total charge of co-ions and counterions residing in the cell was found from the PB calculations to be +24 for the system with the NaCl buffer and +22 for the system with the KCl buffer, compared with the −30 charge of the DNA segment. Fitting the calculated PB charge distributions in accordance with the above power law yields the exponents $\gamma = 1.75$ and $\gamma = 1.98$ for Na^+ and K^+ ions, respectively, in agreement with theoretical predictions.[26] This agreement suggests that the Cl^- ions are mainly located beyond the primary cell in the PB calculations, far from the DNA oligomer, somewhat analogous to the salt-free regime considered in ref 26. Indeed, our PB calculations indicate that only ∼7 chloride ions are located in the vicinity of the DNA oligomer within the primary cell. On the other hand, the additional Cl^- ions (14 overall) confined within the periodic cell in the MD simulations significantly perturb the counterion distribution far from the DNA surface compared with the PB results. We elaborate below how these extra Cl^- ions differently affect the sodium and potassium condensation around DNA.

The above analysis suggests that the PB theory misses many important details of the counterion charge distribution around the highly charged DNA molecule at physiological salt concentrations. First, to reproduce even the long-range charge distribution, which one would have expected to be well described from the PB calculations, requires a careful treatment of the boundary conditions and the finite DNA concentration effect. As suggested in the Introduction, this indicates a limitation on the PB theory-based approaches to treating the electrostatic interactions between linker DNA segments in compact chromatin fibers. Second, the mean-field electrostatics does not properly distinguish between chemically different monocations. The distributions for Na^+ and K^+ coincide after 6 Å from the DNA surface within the PB theory, whereas the MD simulations indicate a prominent difference in the long-range behavior. Thus, the PB theory may be inadequate for addressing the important biological question of which monovalent cation is more effective in mediating DNA compaction.

3.2. Discreteness of Water and Ions. The comparison with the conventional electrostatic picture suggests that the discrete nature of the ions and water plays an important role. In particular, unequal distribution of two ions carrying the same +1 charge originates from their different sizes and their correspondingly different interactions with discrete water molecules. It is well known that, although Na^+ is smaller than K^+, its hydration radius is larger[59,60] because of its larger surface charge density. Since it was suggested that ions with smaller hydration radii have more favorable electrostatic interactions with DNA,[61] the present picture of preferential binding of the Na^+ ions is unexpected.

To understand this effect, we analyze the first peaks of the sodium−DNA and potassium−DNA RDFs from our MD simulations (Figure 4). Overall, the mean positions of the Na^+ and K^+ RDF peaks are shifted with respect to each other because of their different ionic radii. The ions contributing to the first peak approach the immediate vicinity of the polyion such that they are partially or even fully dehydrated. Dehydration can partially explain the higher absorption of Na^+ on DNA: the Na^+ ions are smaller when dehydrated, thus facilitating their infiltration between strands of DNA oligomers and promoting long residence times. This picture is in agreement with prior experimental and theoretical papers, where long residence times for Na^+ ions were found in the minor groove of DNA.[13,15] However, binding of cations in the DNA internal pockets is not the only contribution to the first RDF peak, and additional

(59) Kielland, J. *J. Am. Chem. Soc.* **1937**, *59*, 1675−1678.
(60) Volkov, A. G.; Paula, S.; Deamer, D. W. *Bioelectrochem. Bioenerget.* **1997**, *42*, 153−160.
(61) Ivanov, V. I.; Minchenkova, L. E.; Schyolkina, A. K.; Poletayev, A. I. *Biopolymers* **1973**, *12*, 89−110.

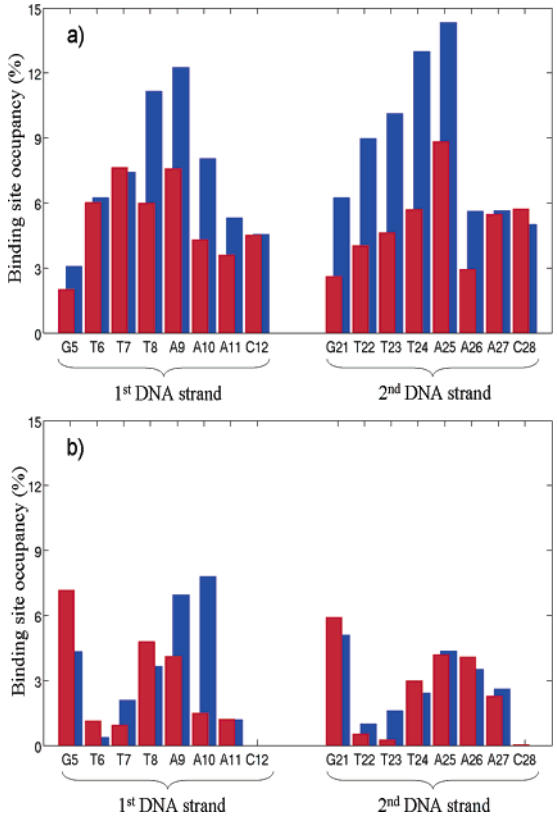

Figure 5. Binding site occupancy (%) of Na^+ (blue) and K^+ (red) for external (a) and internal (b) DNA atoms. Histograms are calculated from simulations **1** and **2** for eight internal DNA base pairs, as explained in the Method section.

ion−DNA contacts contribute as well, as discussed (see also Supporting Information). The DNA−counterion binding site occupancy, calculated from simulations **1** and **2**, provides useful details on the nature of direct counterion binding to DNA (see Figure 5). Sodium binding to phosphates is highly non-uniform, whereas potassium is distributed more evenly (Figure 5a), in agreement with the previous study on Na^+ and K^+ binding to DNA.[32] Phosphate group atoms (O1P, O2P) are associated with the counterions for at least 2−3% of the total simulation time, similar to observations in the prior work.[32] The highest occupancies for both counterions (12−14%) were found at the A25/T8(O1P) central base pair, which may be rationalized by the DNA segment electrostatic potential distribution. It can be seen from Figure 5b that direct binding to the internal DNA sites also takes place; however, it has rather non-uniform character in both simulated systems. A10(N7) and G5(O6) appeared to be the internal sites most occupied by Na^+ (8.5%) and K^+ (7.5%) ions, respectively. Note that, while all phosphates are extensively occupied by both counterions, Na^+ and K^+ have quite different binding patterns for internal DNA sites. This fact confirms the assumption that ionic binding to phosphates is mainly electrostatically driven, whereas the penetration of the DNA core and binding to the internal sites is reminiscent of chemisorption. The contributions of both the external and internal sites binding to the first counterion−DNA RDF peak are larger for Na^+ than for K^+; however, the overall difference is dominated by the electrostatically driven external binding.

While direct binding is determined mainly by the ionic size and the propensity for dehydration, the amplitude and shape of the second peaks, corresponding to water-mediated interactions, cannot be explained by the unequal dehydration propensities. Why is the DNA−K^+ distribution more diffuse, and why do the K^+ ions appear less attracted to the DNA electrostatic field (Figure 4)? We conjecture that the K^+ ions are better screened by the negative Cl^- ions, which are also part of the ionic buffer. To verify this hypothesis, we examined the counterion distributions around the DNA segment from simulation **3**, which consisted of a system with an equal mixture of Na^+ and K^+ counterions and the corresponding NaCl and KCl salts. In this competitive binding simulation, the dissimilar condensation of Na^+ and K^+ is very pronounced (Figure 4c). The presence of both monocations in the system results in a much higher DNA selectivity between the two ionic species. A simple visualization of the MD trajectory confirmed our assumption that negative Cl^- ions interact differently with the Na^+ and K^+ ions. We observed a formation of the constantly broken and re-formed K^+−Cl^- clusters comprised of several K^+ and Cl^- ions. Similar Na^+−Cl^- clusters have not been observed. K^+−Cl^- clustering effectively screens the K^+ ions from the DNA electrostatic field, implying more efficient interaction of the Na^+ ions with DNA. Consequently, whereas the smaller hydration radius of K^+ might imply a higher binding potential with respect to DNA, its complexation with Cl^- counteracts this effect.

To elucidate qualitatively the influence of Cl^- ions on the behavior of Na^+ and K^+ ions, we constructed the counterion−DNA RDFs from simulation **4**, where the NaCl and KCl buffers were removed. As expected, the condensation of both counterions is stronger in the chloride-free system (Figure 4d). The comparison of the Na^+/DNA and K^+/DNA RDFs from simulation **3** (with Cl^-) and simulation **4** (without Cl^-) is shown in Figure 6. Although simulated systems **3** and **4** have unequal overall numbers of counterions, it is reasonable to compare their counterion−DNA RDFs, since the ionic concentration directly enters into the RDF expression (see eq 1). We observe that removing Cl^- ions strongly affects the K^+ ion condensation, whereas the distribution of the Na^+ ions was less perturbed. In particular, Cl^- elimination resulted in the broader DNA−K^+ RDF peak enhancement (the K^+ condensation almost uniformly increased at distances less than 8 Å from the DNA oligomer), while the changes in the DNA−Na^+ RDF were more narrowly localized. Additional striking evidence of the dissimilar chloride−counterion interactions is given by comparing the Na^+−Na^+ RDF with the K^+−K^+ RDF with (Figure 7a) and without (Figure 7b) extra NaCl and KCl salts. A very strong peak in Figure 7a indicates that Cl^- ions induce K^+ ions to co-localize at an average distance of 5 Å from each other, indicating potassium chloride clustering. Exclusion of Cl^- from the system leads to the diffuse K^+ distribution, similar to that observed for the Na^+ ions (Figure 7b).

A visual demonstration of the counterion localization during simulation **3**, the system composed of the mixture of both Na^+ and K^+ counterions and the corresponding salts, is given in Figure 8. The regions of high counterion density, which corresponds to more than 80% of the maximum ion density in a simulation box, are shown. A grid spacing of 1 Å was used. It is seen that sodium condensation greatly dominates in the vicinity of the DNA segment compared with the potassium condensation. The difference between the density distributions for Na^+ and K^+ ions, shown in Figure 8, reflects the most

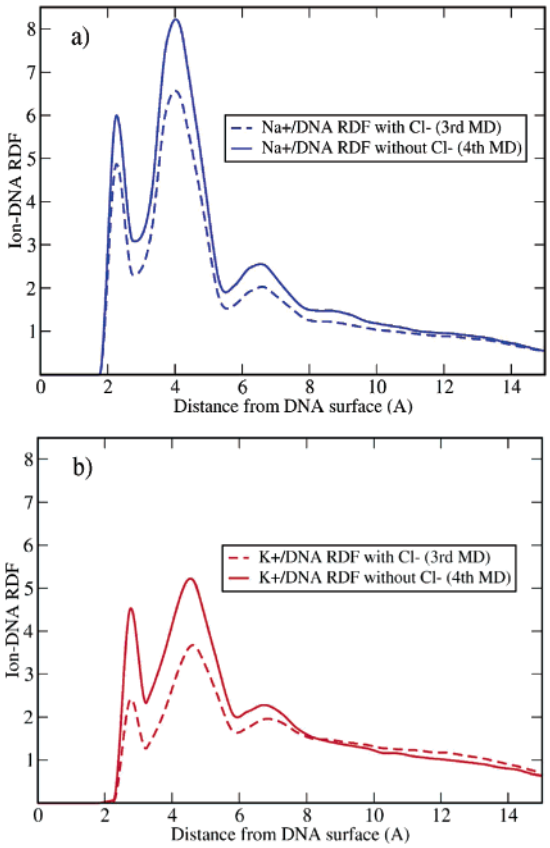

Figure 6. Na^+/DNA (a) and K^+/DNA (b) RDFs from MD **3** with Cl^- (dashed curves) and from MD **4** without Cl^- (solid curves).

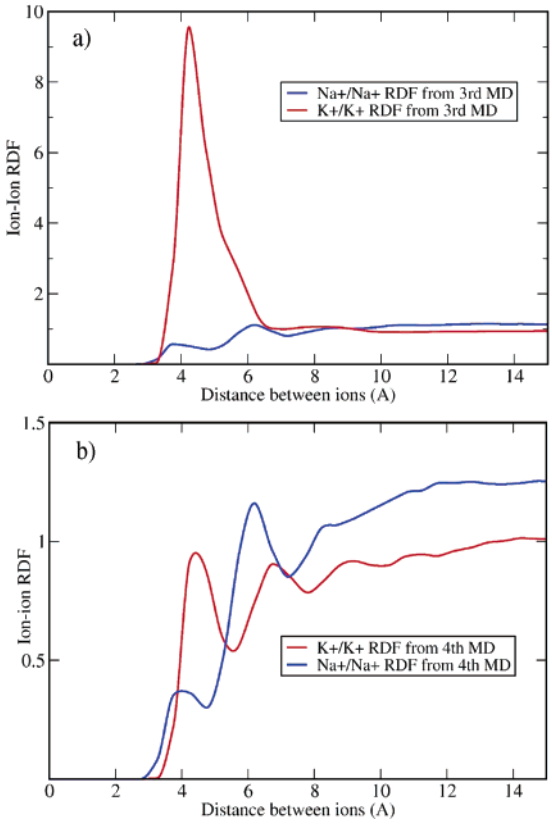

Figure 7. Na^+-Na^+ (blue) and K^+-K^+ (red) RDFs from (a) MD **3** with Cl^- ions and (b) MD **4** without Cl^- ions.

pronounced DNA selectivity among two counterions from our MD simulations (cf. RDFs in Figure 4a,c,d).

In summary, we suggest that three mechanisms are responsible for the observed dissimilarity of Na^+ and K^+ distributions around DNA: (1) smaller Na^+ ions can penetrate the DNA core more easily; (2) smaller Na^+ ions approach closer to the DNA surface and experience larger attractive electrostatic potential; and (3) different polarization of water leads to a higher dehydration penalty for Na^+ and, thus, remarkably less complexation of sodium by Cl^-, resulting in less efficient electrostatic screening. All three effects work cooperatively to enhance Na^+ condensation compared to K^+. To further quantify the relative importance of these effects, we carried out quantitative analysis of the counterion water shell distributions and the counterion−co-ion clustering.

3.3. Ionic Solvation Shell Analysis and Ionic Cluster Distribution. Following the technique described in the Computational Methods section, we constructed solvation curves for the Na^+ and K^+ ions (see Figure 9) that indicate the number of water molecules in the first solvation shell of the counterions as a function of counterion distance from the DNA oligomer surface. As the ions move closer to the polyion, the number of water molecules in their first solvation shell increases (Figure 9). In the systems with pure ionic composition (simulations **1** and **2**), this tendency is much more pronounced for the potassium ions, which acquire approximately two extra water molecules while approaching the DNA segment (see Figure 9a). In contrast, the Na^+ solvation shell remains almost unperturbed by the DNA chain, except in the immediate vicinity of the DNA oligomer, as the Na^+ ions approach the DNA surface. In the

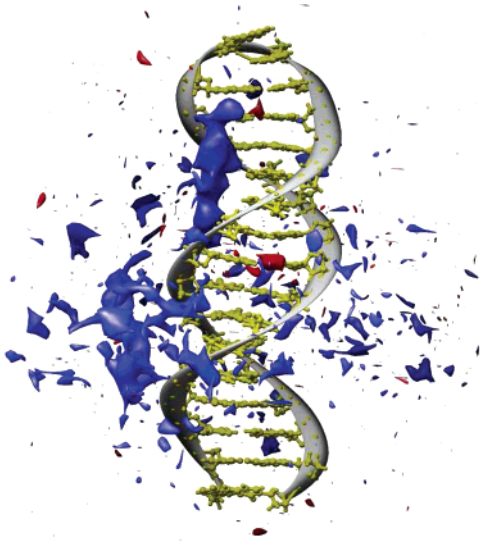

Figure 8. Distributions of Na^+ (blue) and K^+ (red) ions around an average DNA structure, obtained by superposition of all snapshots of MD **3**. The ionic locations shown correspond to >80% of the maximum ion density.

mixture of monovalent ions (simulation **3**), the sodium solvation curve undergoes only minor changes relative to simulation **1**, whereas the potassium curve becomes flatter (Figure 9b). Finally, after exclusion of the extra NaCl and KCl salt from the system, thus removing the Cl^- co-ions, the number of solvent molecules in the first solvation shells of both ion species becomes roughly constant at distances >5 Å from the DNA surface (simulation **4**, see solid curves in Figure 9b).

It seems reasonable to attribute the steep increase in K^+ water coordination as K^+ approaches DNA mainly to electrostatically

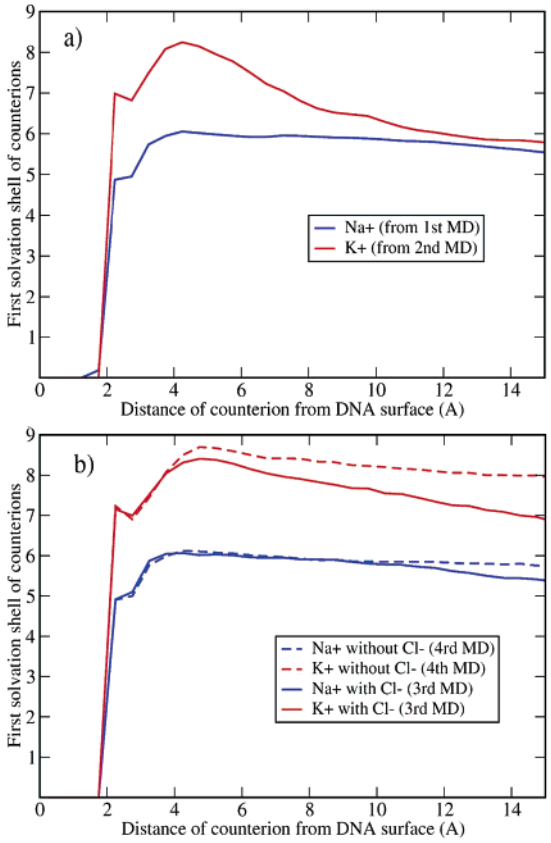

Figure 9. First solvation shells of the Na^+ (blue) and K^+ (red) ions as a function of the ion's distance from the DNA surface, calculated from (a) simulations **1** and **2** and (b) simulations **3** (with salt, dashed curves) and **4** (without salt, solid curves).

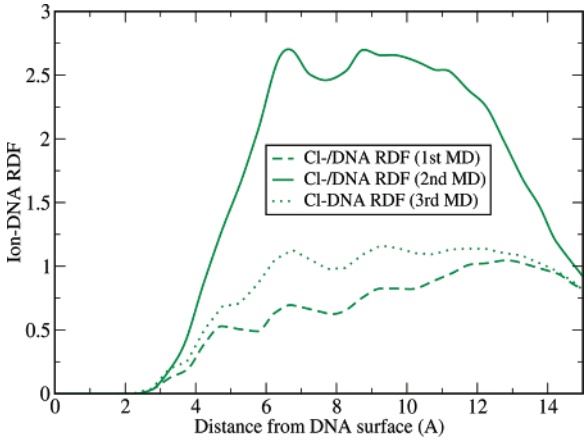

Figure 10. Cl^-/DNA RDFs from simulations **1** (dashed line), **2** (solid line), and **3** (dotted line), corresponding to simple Na^+/NaCl, K^+/KCl compositions and to 1:1 mixture of Na^+/K^+ counterions and NaCl/KCl salts, respectively.

based exclusion of Cl^- from the DNA chain vicinity. Consequently, K^+-Cl^- clustering is expected to diminish near the DNA surface, allowing free K^+ ions in the vicinity of DNA to complete their first solvation shell. To examine this hypothesis, we computed the Cl^-/DNA RDFs in simulations **1**, **2**, and **3**. Surprisingly, we found that the Cl^- ions occupy most extensively the region 2−15 Å from the DNA surface in simulation **2** (see Figure 10), which is the system with the highest clustering. On the other hand, the co-ion profile around DNA obtained from simulation **1** is in agreement with the previously reported Cl^-/DNA RDF,[43] producing a Cl^- concentration smaller than the bulk value at distances of 12 Å or less from the DNA surface (Figure 10). An intermediate chloride distribution emerges from simulation **3**, which contained a mixture of Na^+ and K^+ (Figure 10). Cl^- penetrates the condensed layer of counterions around DNA in all studied systems. This behavior differs from the earlier theoretical prediction,[62] stating that a single peak of co-ion concentration lies just outside the condensed layer of counterions. The K^+-Cl^- clustering results in a chloride distribution which is qualitatively different from the distribution expected from the Poisson−Boltzmann continuum analysis.

The numbers of Cl^- ions within 15 Å from the DNA internal segment surface (see Figure 2b) are 3.3 and 7.0 in simulations **1** (containing only Na^+ ions) and **2** (containing only K^+ ions), respectively. The former number is in agreement with the following simple estimation: the total number $N = 14$ of Cl^- ions in the system multiplied by the ratio $V_{int}/V_{tot} \approx 1/4$ between the volume of interest (see Figure 2b) and the total volume of the system. This gives 3.5 Cl^- ions, which agrees nicely with the 3.3 ions computed from the RDF integration (Figure 10). The latter value is somewhat smaller because of electrostatic repulsion among the DNA and the Cl^- ions. On the other hand, the 2-fold increase obtained from simulation **2** indicates that, in a system with K^+/Cl^- composition, the distribution of Cl^- ions is highly *non-uniform* along the DNA oligomer: the central part of the DNA (eight internal base pairs) is strongly preferred by Cl^-. This may be rationalized by extensive K^+-Cl^- clustering, resulting in electrostatic screening of the negative chloride ions. Consequently, the electrostatic repulsion between DNA and Cl^- is significantly mitigated by cluster formation, allowing Cl^- ions to approach the DNA segment without incurring a large energetic penalty. To examine this effect more closely, we have computed from simulations **2** and **3** the average number of K^+ and Cl^- ions involved in clusters as a function of the distance between the cluster center and the DNA segment surface (Figure 11a,b), as discussed in the Computational Methods section. In addition to these averages, we also obtained histograms showing the full distribution of ions in the clusters, where all clusters were treated on equal footing, regardless of their distance from the DNA (Figure 11c,d).

The obtained distributions indicate that the average cluster charge is *positive* at all distances from the DNA (Figure 11a,b). In this regard, one can think of a cluster as a fictitious positive ion with a fluctuating charge, which interacts with DNA. Variation of cluster charge with distance from the DNA surface indicates a variability of the cluster composition. Indeed, Figure 11b provides insight into the question of why the K^+ ions acquire additional water molecules as they approach DNA (Figure 9). It turns out that the $(K^+_mCl^-_n)$ clusters that are closer to DNA are characterized by a larger difference between m and n ($m \geq n$)—thus the higher positive charge—than the clusters farther away. For instance, it is shown in Figure 3a that a cluster with composition $m = 8$, $n = 5$ (charge +3) is located closer to DNA than an electroneutral cluster with composition $m = 5$, $n = 5$. Consequently, the K^+ ions in clusters with a higher charge contain more water molecules in their first solvation shells because they are coordinated to a smaller degree by the Cl^- ions. This argument rationalizes the monotonically increas-

(62) Ray, J.; Manning, G. S. *Macromolecules* **1999**, *32*, 4588−4595.

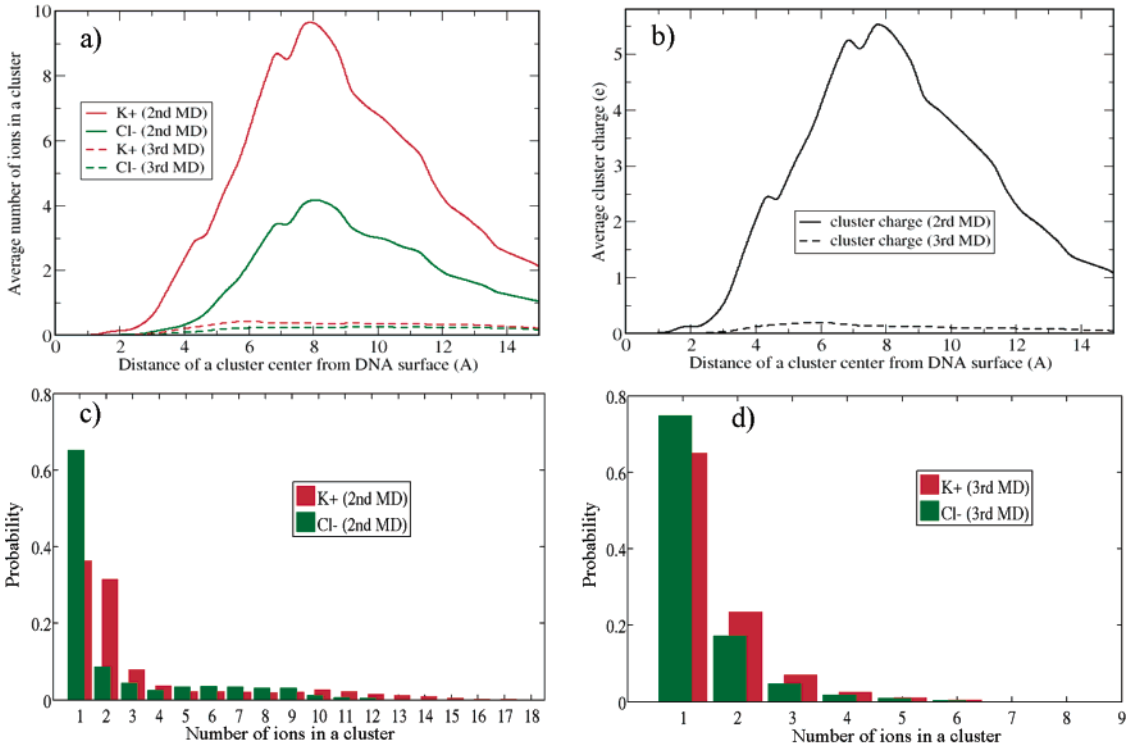

Figure 11. (a) Distribution of cluster ions as a function of distance between cluster center and DNA surface. (b) Distribution of the cluster charge, computed as the difference between K^+ and Cl^- distribution curves (on the left). (c,d) Histograms providing cluster composition.

ing K^+−water curves as the K^+ ions approach the DNA surface (Figure 9). Note that clusters with the highest positive charge are located at 6−7 Å from the DNA (Figure 11b), whereas the peak of a potassium−water curve corresponds to 4−5 Å from the oligomer surface (Figure 9). The positions of these peaks, however, do not have to coincide since the clusters are larger in size compared with the unclustered K^+ ions and the DNA−K^+ interactions start to play a role near the DNA segment.

The more moderate slope of the potassium solvation curve in a mixture of Na^+ and K^+ ions (simulation **3**, Figure 9b) suggests, first, that clustering is not as extensive as in simulation **2**. In addition, both the magnitude of cluster charge and its variation with distance from DNA are much smaller compared with those in simulation **2** (cf. dotted and solid lines in Figure 11b). Indeed, we have found that roughly half of the K^+ (50%) and almost all Cl^- (98%!) ions in simulation **2** are involved in the K^+−Cl^- clusters of various sizes, ranging from 2 to ∼24 of both K^+ and Cl^- ions (Figure 11c). Such a high participation of Cl^- in clustering explains the unexpectedly high chloride residence near the DNA segment (Figure 10). In simulation **3**, on the other hand, only 32% of K^+ and 69% of Cl^- ions are associated in clusters, whose sizes range from 2 to ∼12 K^+ and Cl^- ions (Figure 11d). Interestingly, the dramatic difference between the solid and dashed curves in Figure 11a,b comes from the very different local K^+ and Cl^- concentrations around the internal segment of the DNA chain in systems **2** and **3**. Indeed, the half-as-large K^+ concentration in system **3** compared to system **2**, as well as the 18% lower participation of K^+ in clustering in system **3**, rationalizes this phenomenon. As discussed above (see also Figure 10), high clustering in simulation **2** leads to highly non-uniform distributions of both co-ions and counterions along the DNA, with a tendency for K^+−Cl^- clusters to localize around the central part of the DNA oligomer. In system **3**, however, smaller K^+−Cl^- clusters are distributed more evenly, and the local concentrations of K^+ and Cl^-, participating in clusters, are much lower around the eight internal DNA base pairs, as shown in Figure 11a,b.

Na^+ ions in simulations **1** and **3** tend not to form any clusters with Cl^-. The fraction of the free Na^+ ions is ∼95% in both simulations (histograms not shown). As a result, the Na^+ solvation is much more steady as a function of distance from the DNA oligomer (Figure 9).

In a salt-free system (simulation **4**), there is no counterion clustering for both ions, since bridging Cl^- ions are absent. Both monovalent ions now behave similarly beyond the 8 Å distance from the DNA oligomer (Figure 4d). Although the K^+ ions tend to interact more strongly with DNA when chlorides are removed (see Figure 6), the Na^+ ions still dominate the counterion condensation around DNA. In addition to the differences in the desolvation penalty discussed above, the amplitude of the first counterion−DNA RDF peak is also determined by the size of fully or partially dehydrated ions that are able to penetrate between strands of DNA oligomer and associate with the internal sites of polyion (see the Computational Methods section for the definition of the internal and external DNA sites). The smaller Na^+ ions more readily bind to the polyion internal sites, indicating more favorable Na^+ chemisorption (see Figure 5b). The electrostatic interactions with the external DNA sites also contribute to the first peak. Since the smaller Na^+ ions approach closer to the DNA surface, experiencing stronger attractive electrostatic interactions, this results in enhanced sodium binding to the DNA surface. Therefore, the two main contributions to the first counterion−DNA RDF peak, the chemisorption to the DNA internal sites and the electrostatically mediated condensation to the external DNA sites, both favor stronger Na^+ condensation in all four MD simulations.

Table 1. Number of Ions Contributing to the First Three Peaks of the Ion−DNA RDFs (see Figures 4 and 10) and the Fraction of the Neutralized DNA Charge Computed for All Simulated Systems

	first MD	second MD	third MD	fourth MD
	Na^+ 12.3	K^+ 13.8	Na^+ 6.8	Na^+ 5.8
	Cl^- 0.7	Cl^- 3	K^+ 4.7	K^+ 4.4
			Cl^- 1	
neutralized DNA charge	73%	68%	65%	65%

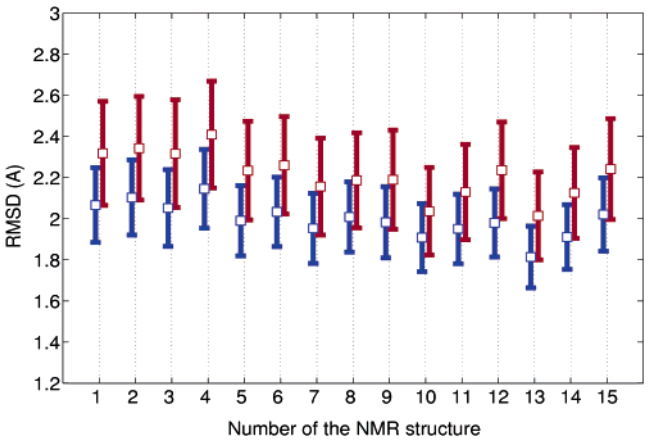

Figure 12. All-atom RMSD of the DNA oligomer of each of the 15 NMR-derived experimental structures[48] for Na^+ (blue) and K^+ (red) salt buffers. Simulations **1** (for Na^+) and **2** (for K^+) were used for calculations.

The remaining difference in the second DNA−counterion RDF peak amplitudes in simulation **4** (no chlorides) may be partially explained by the peak positions: the DNA−Na^+ peak is found to be closer to DNA; thus, the Na^+ atoms experience an enhanced attraction to the DNA electrostatic field. In addition, Na^+ and K^+ lose a different number of water molecules from their first solvation shells when approaching the DNA surface (Figure 9). While the Na^+ ions lose only ∼1 water molecule when approaching a distance corresponding to the second RDF peak position (Figure 4d), indicating water-mediated counterion−DNA interactions, the K^+ ions lose ∼2 water molecules at the second RDF peak position (see the changes in the solvation curves in the range of distances 2.75−4.3 Å for Na^+ and 3.25−5 Å for K^+ from the DNA surface). Thus, the loss of two water molecules from the K^+ solvation shell might be unfavorable compared with a single water molecule loss from the Na^+ solvation shell when ions approach the position of the DNA−counterion second RDF peak.

The number of Na^+, K^+, and Cl^- ions contributing to the first three RDF peaks in simulations **1**−**4**, as well as the fraction of the DNA charge neutralized by the condensed ions, is summarized in Table 1. We have adopted the definition of Beveridge and co-workers[31] for the condensed counterions as those lying within a 9 Å region from the DNA surface, where ions are structured with respect to DNA, as determined by the location of the RDF peaks (Figure 4). The fraction of neutralized DNA charge was predicted to be around 76% by the counterion condensation, Poisson−Boltzmann, and field theories[19,41] and was confirmed by the all-atom MD simulations.[31] We computed this fraction as the difference between the number of counterions and co-ions in the 9 Å region from the DNA surface, divided by 16, which is the total charge of the internal eight base pairs. Interestingly, the value of 73%, very similar to the theoretical prediction, was obtained for simulation **1**. On the other hand, salt-free simulation **4** resulted only in 65% DNA charge compensation. Similar values of 68% and 65% were obtained for simulations **2** and **3**, respectively. Note that a fraction value of 76.5% was reported in a prior MD simulation on the Na^+/NaCl mixture;[43] however, that was within 10 Å from the DNA surface. We attribute the lower fraction values in our simulations **2**−**4**, compared to 76%, to a lower propensity of K^+ to condense around DNA and a larger propensity for the Cl^- ions to penetrate the DNA proximity, due to K^+−Cl^- clustering in simulations **2** and **3**.

3.4. Counterion Modulation of the DNA Conformational Dynamics and Comparison with the Experiment. We compared our MD simulation DNA segment ([d(CGAGGTTTAAACCTCG)]$_2$) snapshots with the experimental results. The 16-base-pair DNA segment investigated in the present paper was studied experimentally by NMR techniques.[48,63] We used the 15 lowest energy structures proposed from the NMR investigation[48] as reference states for calculating the all-atom root-mean-squared deviation (RMSD) of the DNA segment snapshots during simulations **1** and **2**. The obtained average RMSD values and their variances for each of the 15 NMR-derived experimental structures are shown in Figure 12. In general, the calculated mean values and the extents of the fluctuations are consistent with the values reported in prior computational works for DNA 12-mer segments.[27] We observed that both the average RMSDs and the RMSD fluctuations are larger for the K^+ system, indicating that, in a potassium salt environment, the DNA oligomer is more flexible.

This result is rather surprising since Na^+, as discussed earlier, neutralizes DNA much more efficiently, which, in turn, is expected to increase DNA flexibility due to decreased electrostatic repulsion among the DNA base pairs. To explain the observed trend, we conjecture that Na^+ ions, due to their higher penetration of the DNA interior, could rigidify the DNA core, reducing conformational fluctuations.

4. Conclusions

In the present work, we investigated in detail how Na^+ and K^+ are distributed around DNA. These two counterions are among the most commonly used in the experimental studies of DNA fibers and chromatin. We carried out a series of extended all-atom MD simulations of a 16-base-pair DNA oligomer in explicit water and various ionic environments. Long trajectory times (60 ns) and the relatively large size of the DNA segment make our simulations among the largest DNA simulations reported to date. Instead of focusing on sequence-specific details, as is customary in the computational DNA literature, we analyzed the average behavior of both monocations along the *whole* DNA segment at distances up to 15 Å from its surface. Our work was motivated by inconclusive experimental data on whether Na^+ or K^+ condenses more strongly around DNA. Whereas recent NMR measurements[13] suggested a slightly higher affinity for K^+ than Na^+ to bind to the DNA minor groove, the electrophoretic measurements of the DNA chain mobility[34] may be interpreted to suggest the opposite picture. Since similar trends in DNA mobilities were obtained for single- and double-stranded oligomers, with and without an A-tract,[34] the preferential sequence-specific counterion binding in the

(63) Lingbeck, J.; Kubinec, M. G.; Miller, J.; Reid, B. R.; Drobny, G. P.; Kennedy, M. A. *Biochemistry* **1996**, *35*, 719−734.

minor groove probably does not determine the overall outcome of the counterion condensation around the whole DNA segment.

We found that, on average, Na^+ penetrates more of the DNA interior and also condenses more around the DNA exterior compared with K^+. Our results are consistent with the prior electrophoretic measurements,[34] as well as with other experiments on DNA compaction by various monocations.[39] Using several computational analysis techniques, among them methods for computing the counterion−DNA RDFs, counterion−co-ion cluster analysis, and counterion solvation shell analysis, we determined that three distinct mechanisms are responsible for such behavior: (1) smaller Na^+ ions are sterically better fit into the DNA interior sites; (2) smaller Na^+ ions approach closer to the DNA exterior surface, experiencing stronger DNA electrostatic potential; and (3) K^+ forms clusters with Cl^- more readily, due to a smaller dehydration penalty, which, in turn, leads to better electrostatic screening and less K^+ condensation around DNA. Our analysis of the counterion−co-ion clusters showed that roughly half of K^+ is associated with Cl^-, while almost all of Na^+ is cluster-free. We observed and rationalized the increased DNA selectivity between Na^+ and K^+ in the mixture of both counterions, as opposed to systems with either Na^+ or K^+ counterions.

We also compared the all-atom MD DNA−counterion distributions with the mean-field electrostatic results. The PB theory does not capture many important details at short distances from the DNA surface, such as the first counterion−DNA RDF peak, which corresponds to the counterion chemisorption. Somewhat surprisingly, even far from the DNA surface, the counterion charge distributions were different in the MD simulations and in the PB calculations. Dissimilar boundary conditions, corresponding to a finite DNA concentration in the MD simulations and infinitely dilute DNA solution in the PB calculations, were used to rationalize this discrepancy.

Finally, we analyzed the modulation of the DNA oligomer structural dynamics by two monovalent ions and compared it to the experimental results by calculating the RMSDs among the MD trajectory snapshots with 15 NMR-derived models.[48] While the RMSD mean values and the standard deviations are within the range of those obtained in the earlier works,[27] we found that RMSDs are larger in the K^+ buffer, with larger DNA flexibility. In an ongoing work, we are developing ionic-environment-specific coarse-grained models of linker−DNA chains based on the results from the all-atom explicit water MD simulations reported here.

Acknowledgment. We thank Michael Rubinstein and Johan Ulander for stimulating discussions. We are grateful to Nikolay Dokholyan, Lee Pedersen, Michael Rubinstein, and Holden Thorp for reading critically the manuscript and providing helpful comments. This work was partially supported through North Carolina Biotechnology Center (NCBC) grant 2006-MRG-1107.

Supporting Information Available: Table showing the binding site occupancy of counterions for external O1P,O2P phosphate and for internal N7,N3,O2,O6,O4 DNA atoms, computed from simulations **1** and **2**. This material is available free of charge via the Internet at http://pubs.acs.org.

JA0629460